Chapter 13

DECOMPOSITION OF THREE-DIMENSIONAL MAGNETOTELLURIC DATA

Xavier Garcia and Alan G. Jones

Geological Survey of Canada, 615 Booth Street, Ottawa, ON, K1A 0E9, Canada

Abstract: Decomposition of magnetotelluric data into a local galvanic 3D distortion matrix and a regional 2D Earth caused a quantum leap in our understanding of complex data and our ability to handle those data. The Groom–Bailey method is the most widely adopted tensor decomposition approach, and rightly so given its physical basis and its separation of distortion parameters into determinable and indeterminable parts. However, on occasion the 3D over 2D (3D/2D) decomposition fails in that the misfit of the model to the data is far greater than the data errors permit, and this failure is due to either the distortion model being invalid or to inappropriately small error estimates for the data. In this paper we describe and demonstrate our attempts to extend MT tensor decomposition to local galvanic 3D distortion of regional 3D data (3D/3D). There are insufficient data to accomplish this uniquely for a single MT site, so some approximations must be made. The approach we use is to assume that two neighboring sites sense the same regional structure if they are sufficiently close compared to the skin depth to the structure, but that the two sites have differing galvanic distortion matrices. We use a decomposition method similar to the Groom–Bailey one, but with a different parameterization, and we solve the problem using a Newton method. We demonstrate the method to a synthetic data set, and highlight the difficulties that result as a consequence of inherent parameter-resolution instabilities.

1. INTRODUCTION

The presence of electrical charges near electrical conductivity transitions in the Earth cause galvanic distortions of magnetotelluric (MT) data to varying degrees. When such charges occur associated with local, near-surface inhomogeneities there is an inherent spatial aliasing problem which must be addressed prior to interpretation. The basic formulation of galvanic distortion consists of the tensor decomposition of the measured (superscript D) distorted electromagnetic fields ($\boldsymbol{E}$, $\boldsymbol{H}$) into a series of regional fields and distortion matrices (Wannamaker et al., 1984; Habashy et al., 1993; Chave and Smith, 1994):

$$\begin{aligned} \boldsymbol{E}^{\mathrm{D}} &= \boldsymbol{E}\boldsymbol{P}, \\ \boldsymbol{H}^{\mathrm{D}} &= \boldsymbol{E}\boldsymbol{Q}_{\mathrm{h}} = \boldsymbol{I} + \boldsymbol{Q}_{\mathrm{h}}\boldsymbol{Z}, \\ \boldsymbol{H}_{z}^{\mathrm{D}} &= \left[(\boldsymbol{A},\boldsymbol{B}) + \boldsymbol{Q}_{z}\boldsymbol{Z}\right]\boldsymbol{H}, \end{aligned} \tag{13.1}$$

where $\boldsymbol{P}$, $\boldsymbol{Q}_{\mathrm{h}}$ and $\boldsymbol{Q}_{z}$ are real valued and frequency-independent distortion matrices (Jiracek, 1990):

$$\boldsymbol{P}=\begin{pmatrix} P_{xx} & P_{xy} \\ P_{yx} & P_{yy} \end{pmatrix}, \quad \boldsymbol{Q}_{\mathrm{h}}=\begin{pmatrix} Q_{xx} & Q_{xy} \\ Q_{yx} & Q_{yy} \end{pmatrix} \quad \text{and} \quad \boldsymbol{Q}_{z}=\begin{pmatrix} Q_{zx} & Q_{zy} \end{pmatrix}, \tag{13.2}$$

and $(\boldsymbol{A},\boldsymbol{B})$ is the vertical magnetic transfer function or tipper. Thus, the distortion of the regional MT transfer function can be written as:

$$\boldsymbol{Z}^{\mathrm{D}}=(\boldsymbol{I}+\boldsymbol{P})\boldsymbol{Z}\left(\boldsymbol{I}+\boldsymbol{Q}_{\mathrm{h}}\boldsymbol{Z}\right)^{-1}, \tag{13.3}$$

where $\boldsymbol{Z}$ is the general regional impedance, $\boldsymbol{Z}^{\mathrm{D}}$ is the observed impedance, and $\boldsymbol{I}$ is the identity matrix. Similarly, the regional vertical field transfer function is distorted

$$(\boldsymbol{A},\boldsymbol{B})^{\mathrm{D}}=\left[(\boldsymbol{A},\boldsymbol{B})+\boldsymbol{Q}_{z}\boldsymbol{Z}\right](\boldsymbol{I}+\boldsymbol{Q}\boldsymbol{Z})^{-1}, \tag{13.4}$$

where $(\boldsymbol{A},\boldsymbol{B})$ is the regional transfer function and $(\boldsymbol{A},\boldsymbol{B})^{\mathrm{D}}$ is the observed one.

When the EM fields are observed in an arbitrary coordinate system that is not aligned with the strike angle of the regional structures, the observed impedance (Equation 13.3) becomes

$$\boldsymbol{Z}^{\mathrm{D}}=\boldsymbol{R}(\theta)(\boldsymbol{I}+\boldsymbol{P})\boldsymbol{Z}\left(\boldsymbol{I}+\boldsymbol{Q}_{\mathrm{h}}\boldsymbol{Z}\right)^{-1}\boldsymbol{R}^{\mathrm{T}}(\theta), \tag{13.5}$$

where θ is the azimuth angle respect to the regional strike, $\boldsymbol{R}$ is the Cartesian rotation matrix, and superscript T denotes transpose.

Following this basic tensor decomposition, several authors developed different approaches to extract the regional impedances given the observed ones (Larsen, 1977; Groom and Bailey, 1989; Bahr, 1991; Zhang et al., 1993; Chave and Smith, 1994; Smith, 1997).

Most of the authors neglect galvanic magnetic distortion. The reason for this lies in the fact that the magnetic distortion in Equation (13.3) is $\boldsymbol{Q}_{\mathrm{h}}\cdot\boldsymbol{Z}$, rather than $\boldsymbol{Q}_{\mathrm{h}}$ alone which describes the scattering. This product term is frequency-dependent, due to the frequency dependence of $\boldsymbol{Z}$, and vanishes for low frequencies. For this reason magnetic galvanic distortion is usually ignored. Jones and Groom (1993), Chave and Smith (1994) and Smith (1997) account for the magnetic term in their galvanic distortion of MT data, and Ritter and Banks (1998) consider the effects on the vertical field transfer functions. For distortion of controlled-source data there is the theoretical work of Qian and Pedersen (1992), while Li et al. (2000) study the anisotropy case, and Garcia et al. (2000) provide a case study of controlled-source data in which the magnetic distortion is taken into account.

The most widely used decomposition technique is the one proposed by Groom and Bailey, 1989 (called GB). Two angles, *twist* and *shear*, describe the galvanic distortion of the regional electric field. There are two other distortion parameters, *local anisotropy* and *site gain*, that are unresolvable amplitude scaling effects and are included in the regional impedance matrix. The anisotropy can be approximated by assuming that the asymptote of the apparent resistivity curves for both off-diagonal terms for the high frequency should be coincident. The remaining distortion parameter, site gain, is usually small and can be addressed using either additional geophysical or geological information or determined as part of the inversion procedure.

When applying MT for addressing mining scale problems, the frequencies of interest range from approximately 1 Hz to 20,000 Hz. Within the depth of penetration corresponding to this frequency band most mineralized structures will show 3D inductive effects, and existing decomposition schemes are not valid as they assume regional 1D or 2D Earth models. The first attempt to deal with distortion over 3D regional structures was that of Ledo et al. (1998), who assumed a 3D/2D/3D Earth, with the upper 3D structures causing the galvanic distortion. Following their approach, conventional Groom–Bailey decomposition is performed at high frequencies, where the regional structures can be considered 2D. Then they apply the derived distortion parameters to the data over the whole observational frequency range. Recently, Utada and Munekane (2000) presented a 3D/3D decomposition method that makes use of the spatial derivatives of the magnetic fields to estimate galvanic distortion. Their method requires a large number of stations located in a 2D array, and measurement of the vertical magnetic field at each site. Both of these are not common practice in mineral exploration MT surveys.

In the present work we discuss our attempts to extend galvanic decomposition of the electric field to 3D regional Earth models. Two theoretical data sets are examined and decomposed using our approach, with varying degrees of success due to the inherent instabilities of the problem as posed. We conclude that this approach may prove fruitful, but that further work is required.

2. 3D DECOMPOSITION

Figure 1 shows a generalized model of galvanic and inductive interactions at a variety of depths and scales. The electromagnetic spectrum can be separated into four different bands depending on the effects observed. At the highest frequencies the shallow surficial

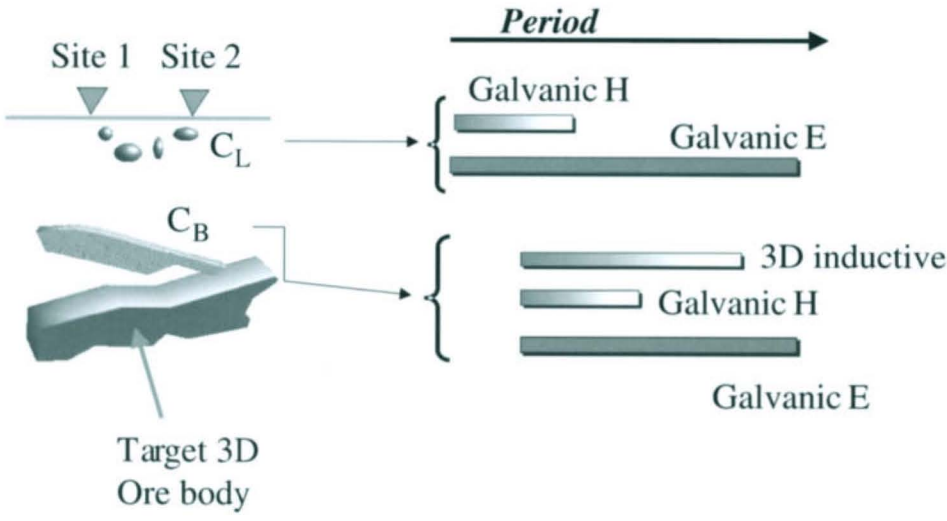

Figure 1. Cartoon of the different inductive and galvanic effects that appear in a MT mining scale survey.

inhomogeneities are the only source of galvanic distortion effects, and these can be described by a distortion tensor, $\boldsymbol{C}_{\mathrm{L}}$. At lower frequencies the 3D distorting structures, if sufficiently elongate, will have a response that can be characterized as 2D. As the frequency decreases (and penetration depth increases) the 3D inhomogeneity causes 3D inductive effects. At the lowest frequencies only the galvanic distortion of both the surficial ($\boldsymbol{C}_{\mathrm{L}}$) and distorting body ($\boldsymbol{C}_{\mathrm{B}}$) of the electric fields will remain, and a classical GB scheme could be applied to retrieve the combined distortion parameters $\boldsymbol{C}$. For even lower frequencies the 3D inductive and galvanic effects from the 3D regional structure, the mineralized ore body, appear in the response curves. In this frequency range of interest, the distorted impedance can be decomposed into two inseparable distortion matrices and a regional 3D response:

$$\boldsymbol{Z}^{\mathrm{D}} = \boldsymbol{C}\boldsymbol{Z} = \boldsymbol{C}_{\mathrm{L}}\boldsymbol{C}_{\mathrm{B}}\boldsymbol{Z}, \tag{13.6}$$

where $\boldsymbol{C}_{\mathrm{L}}$ is the distortion caused by the shallow structures, $\boldsymbol{C}_{\mathrm{B}}$ the distortions caused by the 3D structure, $\boldsymbol{C}$ is their combined effect, and $\boldsymbol{Z}$ the regional 3D response. We wish to determine the 3D impedance of the mineralized body, $\boldsymbol{Z}$, given the observations $\boldsymbol{Z}^{\mathrm{D}}$, and therefore need to extract the parameters of $\boldsymbol{C}$.

Given that only eight equations are obtained for each frequency from the observed impedance tensor for each station, and that the 3D distortion problem described by Equation (13.6) has 12 unknowns (4 complex impedances plus 4 distortion parameters), an approximation is required in order to solve the problem. We assume that two adjacent stations respond to the same 3D regional response $\boldsymbol{Z}^{\mathrm{D}}$ but different local galvanic effects, C^1 and C^2. This assumption reduces the problem to $16 \times N$ equations and $8 \times N + 8$ unknowns (4 impedances $\times$ 2 (complex) $\times$ N frequencies + 4 distortion parameters $\times$ 2 stations) for N frequencies, and the problem may have a solution.

This approach is limited to situations where the distortion parameters are different at both sites but the regional parameters are the same. In the case of both stations being affected by the same galvanic distortion their responses should be identical (to within statistical error), then the problem has no solution as the real number of equations will be smaller than the number of parameters.

3. DECOMPOSITION ALGORITHM

Two different approaches have been applied to address this problem. The first one was to consider the distortion parameters as described in Equation (13.6), then the impedances recorded at two nearby sites can be rewritten as:

$$\begin{aligned} Z^{\mathrm{D},1} &= \begin{pmatrix} C_1^1 & C_2^1 \\ C_3^1 & C_4^1 \end{pmatrix} \begin{pmatrix} Z_{xx} & Z_{xy} \\ Z_{yx} & Z_{yy} \end{pmatrix}, \\ Z^{\mathrm{D},2} &= \begin{pmatrix} C_1^2 & C_2^2 \\ C_3^2 & C_4^2 \end{pmatrix} \begin{pmatrix} Z_{xx} & Z_{xy} \\ Z_{yx} & Z_{yy} \end{pmatrix}, \end{aligned} \tag{13.7}$$

where the superscript index refers to each site.

For this form, two different least-squares algorithms have been tried; one based on a Marquardt–Levenbergs scheme (Pedersen and Rasmussen, 1989) and the second using a

sequential quadratic programming method as implemented in the NAG [1] libraries. Both methods failed to solve the problem, and an inspection of the matrices revealed that the condition number was of the order of around 80, which is too big for the accuracy required to reach a minimum and invalidated the use of such algorithms.

The second description used was similar to the GB approach (Groom and Bailey, 1989), where the impedances for two neighboring sites can be decomposed and rewritten as:

$$
\begin{aligned}
Z^{\mathrm{D},i} &= g^i T^i S^i A^i Z \\
&= \begin{pmatrix} 1 & -t^i \\ t^i & 1 \end{pmatrix} \begin{pmatrix} 1 & s^i \\ s^i & 1 \end{pmatrix} \begin{pmatrix} g^i(1+a^i) & 0 \\ 0 & g^i(1-a^i) \end{pmatrix} \begin{pmatrix} Z_{xx} & Z_{xy} \\ Z_{yx} & Z_{yy} \end{pmatrix} \\
&= \begin{pmatrix} 1 & -t^i \\ t^i & 1 \end{pmatrix} \begin{pmatrix} 1 & s^i \\ s^i & 1 \end{pmatrix} \begin{pmatrix} g_1^i & 0 \\ 0 & g_2^i \end{pmatrix} \begin{pmatrix} Z_{xx} & Z_{xy} \\ Z_{yx} & Z_{yy} \end{pmatrix}, \qquad i = 1,2. \qquad (13.8)
\end{aligned}
$$

We studied various parameterizations of this equation, including those of Groom and Bailey (1989) and of Chave and Smith (1994). The classical distortion decomposition parameterization of Groom and Bailey (1989) was based on the Pauli matrices, and is a natural one for decomposition of a tensor with only elements on the diagonals or off-diagonals. When testing with the GB parameterization we found the algorithm to be highly sensitive to start model and to deviate rapidly to local minima.

Of the forms that we tested, the parameterization that yielded the greatest stability was to solve for a new set of complex functions α_i defined in the following way:

$$
\begin{aligned}
\alpha_0^i &= \frac{Z_{xx}^{\mathrm{D},i} - Z_{yx}^{\mathrm{D},i}}{2}, \qquad \alpha_1^i = \frac{Z_{xx}^{\mathrm{D},i} + Z_{yx}^{\mathrm{D},i}}{2}, \\
\alpha_2^i &= \frac{Z_{xy}^{\mathrm{D},i} - Z_{yy}^{\mathrm{D},i}}{2}, \qquad \alpha_3^i = \frac{Z_{xy}^{\mathrm{D},i} + Z_{yy}^{\mathrm{D},i}}{2}, \qquad i = 1,2. \qquad (13.9)
\end{aligned}
$$

In our new parameterization every α_i depends only on two regional impedance elements instead of four as required by the classical GB one. Each α_i is more sensitive to the parameters that form it, which accounts both for their sensitivity and for the stability.

To solve this system of equations we used a Newton algorithm to find the minimum of the square of the norm between the estimated impedance and the measured impedance:

$$
\mathrm{fn} = \sum_j \left(\alpha_j^0 - \alpha_j^{\mathrm{m}}\right)^2, \qquad (13.10)
$$

where α^0 are the data and α^m are the model parameters defined according to Equation (13.9). As we will see later, different tests performed on synthetic data were successful in retrieving the regional response together with the distortion parameters.

The misfit that we use is a χ-square misfit:

[1] NAG: Numerical Algorithms Group, Fortran 77 mathematical libraries, version 17. The specific library use in this work is E04KDF, that is a modified Newton algorithm.

$$\mathrm{RMS} = \sqrt{\sum_j \left(\frac{\alpha_j^0 - \alpha_j^{\mathrm{m}}}{\delta \alpha_j^0} \right)^2}, \qquad j = 0, \ldots, 3, \tag{13.11}$$

where α_j^0 are the data and α_j^{m} are the model responses, and $\delta \alpha_j^m$ are the data variances.

4. SYNTHETIC TESTS

We discuss below two tests using synthetic data that illustrate the reliability and limitations of our approach. We derived the theoretical responses at an MT station above a three-dimensional (3D) resistivity model, shown in Figure 2, using Randy Mackie's 3D forward modelling code (Mackie et al., 1994). The model consisted of a moderately conductive exposed medium (100 Ω m), a dipping resistive structure (2000 Ω m) at depth, and a conductive (5 Ω m) elongated structure that crosses the two media at an angle of 45°. The grid used was of 105 × 105 × 50 cells, with a minimum grid size in X and Y of 250 m and in Z of 90 m. Responses at a total of 11 frequencies were calculated from 10^{-3} to 10^2 Hz. The scaled impedances for the station located in the center of this model are shown in Figure 3. These synthetic responses were perturbed using two sets of distortion parameters (listed in Table 1), and Figure 4 shows the responses of the two stations obtained in this way. For both tests we assumed that the data had associated errors of 2% of their impedance amplitudes.

Previous to any three-dimensional decomposition we proceeded to decompose both stations using a 2D algorithm (McNeice and Jones, 2001). As both stations have the same response with different galvanic distortion, we expect that the final 2D decomposed data should be the same, but different twist and shears. The results corresponding to the decomposition of both sites simultaneously are presented in Figure 5a for station 1 and Figure 5b for station 2. The error in interpreting these data is clearly shown in these figures (left upper corner panel). Besides that the error misfit is too big to be considered a good fit, the regional responses (middle right panel) are totally different and the program could not retrieve the distortion parameters (bottom left panel).

The results we present below consist of the decomposition of an impedance tensor at four frequencies, both with the gains fixed and with them free. Different tests were undertaken using different numbers of frequencies and different distortion models, and the results were essentially the same.

Table 1. Distortion parameters used to obtain stations 1 and 2 used in the present work [a]

Station 1		Station 2	
g1 = g_1^1	0.9	g3 = g_1^2	1.43
g2 = g_2^1	0.9	g4 = g_2^2	1.43
t1	−20°	t2	−5°
s1	35°	s2	−17°

[a] If the anisotropy is zero, then the gain factors in each station are equal.

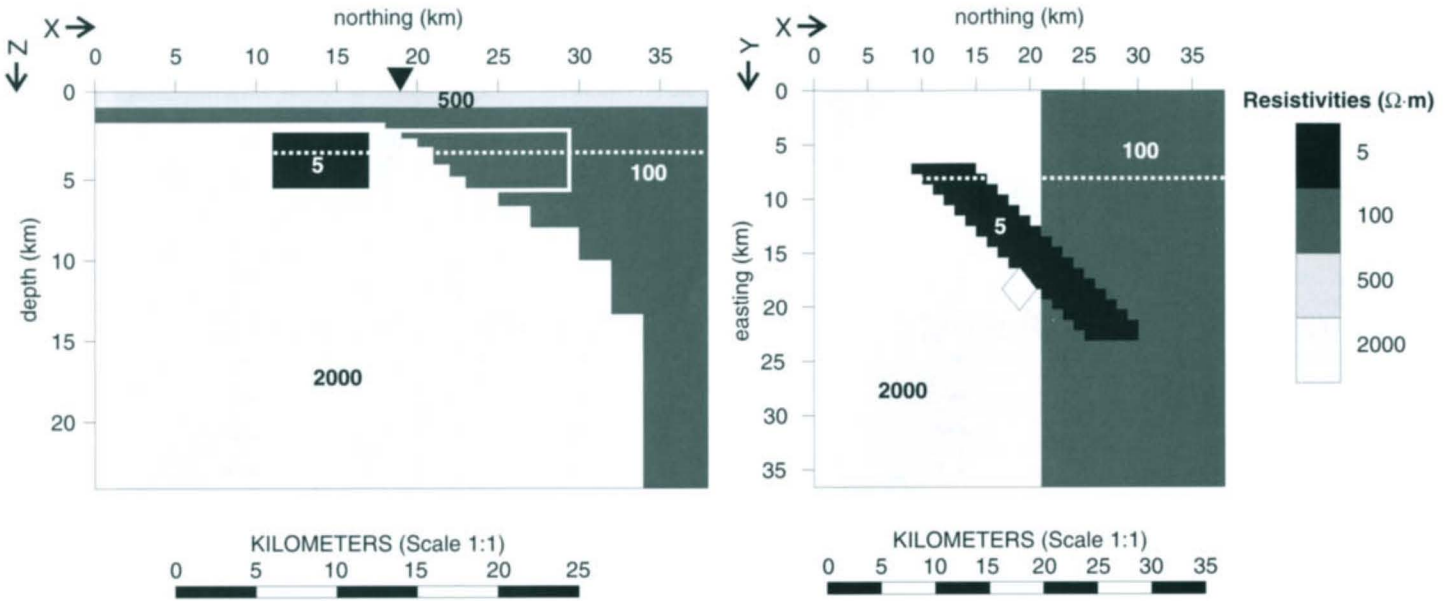

Figure 2. Theoretical regional model used in this study. It consists of a 100-Ω m background with an embedded resistive structure dipping towards the *X* direction, and a conductive structure crossing the model at 45°. We calculate the responses of this model using Randy Mackie's 3D forward modelling code. The white box on the right indicates the extent of the conductor. The white dotted lines indicate the position of the slices.

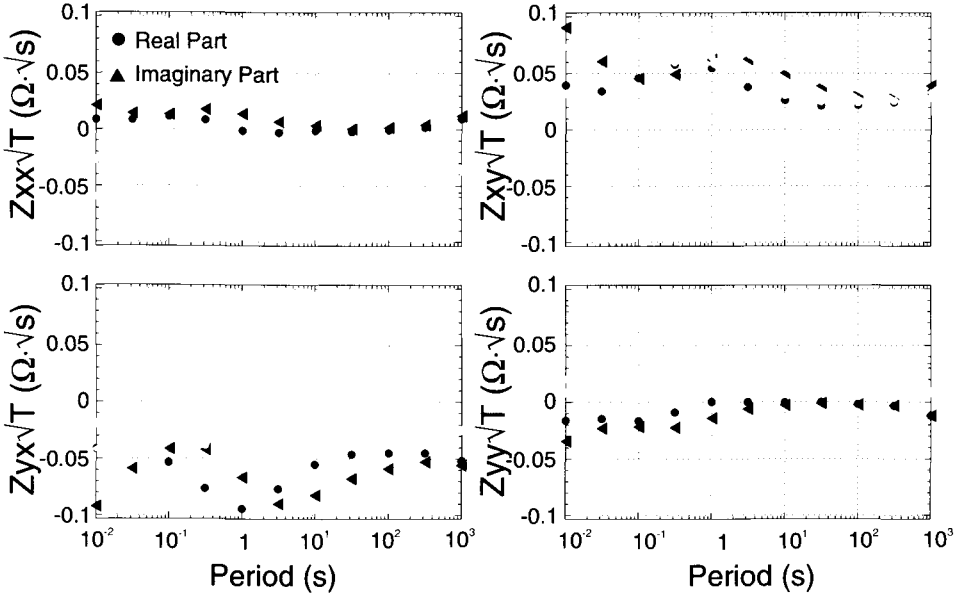

Figure 3. Impedance tensor scaled by the square of the period, obtained from the theoretical model in Figure 2. This is the regional response used in this study.

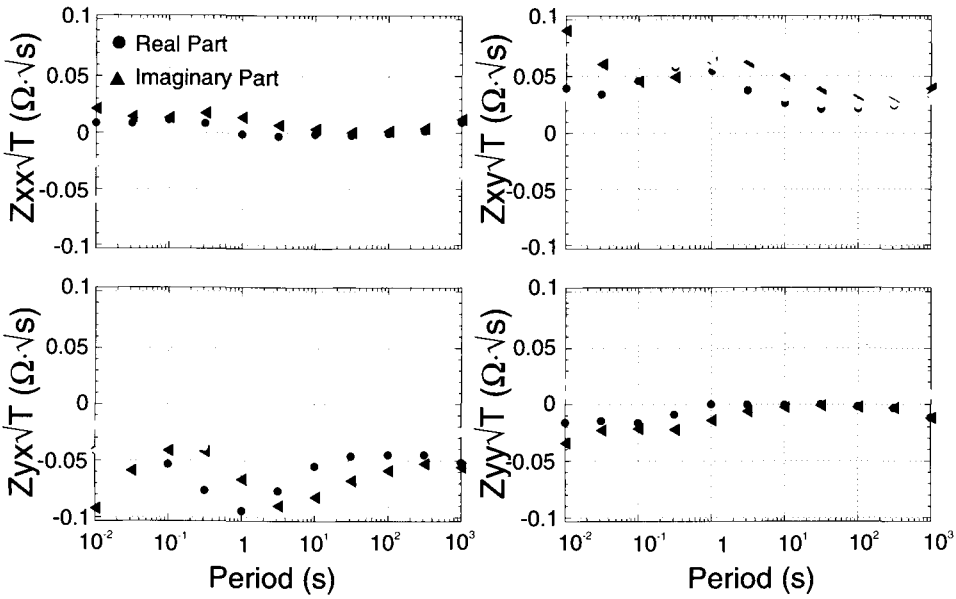

Figure 4. Impedances scaled by the square of the period corresponding to the two stations obtained applying distortions parameters (Table 1) to the station from the 3D model. In gray there is station 1 and the black responses are station 2.

4.1. Example 1: Gains fixed

In this first test we held the gain parameters fixed to their actual values. Figure 6a shows the decrease of RMS misfit with successive iterations. For this case convergence was rapid and within 10 iterations a satisfactory solution was achieved with an RMS misfit of 0.6972. As an example of convergence of the parameters to their correct values we show the evolution of the shear and twist angles (Figure 6b) and the impedance elements Z_{xy} and Z_{yx} (both real and imaginary parts) at a frequency of 122.1 Hz (Figure 6c) as the iterations increased. The correct values are indicated in Figure 6b,c, and an excellent agreement between the determined parameters and the actual ones is apparent. We can conclude that if we know a priori the gain parameters, we can recover the other distortion parameters to within statistical accuracy.

4.2. Example 2: All parameters free

For the second example we demonstrate decomposition of the same data but with the gain parameters free in an attempt to recover them. For the initial tests the twist and shear angles at both sites were held fixed to their true values. The final solutions recovered the correct impedances and the gain parameters after six iterations.

However, the real challenge is decomposition of the data with all parameters unconstrained. Figure 7a shows the evolution of the misfit function for successive iterations, with a final RMS misfit of 0.9265 after 10 iterations. The twist angles at both sites have been recovered after few iterations (Figure 7b) and the shear angles are close to their correct values (Figure 7b). However, the impedances (Figure 7d) and gains (Figure 7c) are significantly different from their correct values. Nevertheless the final decomposed model fits the data to within statistical tolerances (RMS misfit < 1.0), but the final parameters are far from the correct solution. Figure 8 shows the actual regional scaled impedances compared to those derived using the above final solution. As can be observed, the fit is better at high frequencies showing a constant shift at lower frequencies. As stated above in the Introduction, there is a strong equivalence problem that must be solved using additional geological and geophysical information, just as in the GB case for solving for the unknown site gain and anisotropy parameters.

The main problem associated with this method is that the gain parameters appear to be virtually impossible to recover from the distorted impedances. Including the gain factors into the decomposition, as undertaken in the Groom–Bailey method, results in two differently scaled regional parameters, and the parameters to obtain will be $16 \times N + 4$ instead of the prior $8 \times N + 8$, making the problem impossible to solve.

To study this equivalence problem we undertook an analysis consisting of a series of realizations obtained by adding 1% Gaussian noise and scatter to the impedance tensor elements of the two distorted stations. These individual realizations were each decomposed, and the results demonstrated that the problem is sensitive to small departures. A statistically satisfactory fit (RMS misfit < 1.0) can be achieved for each realization, but the 3D regional impedance parameters are not correctly recovered. As an example of the poor sensitivity of the individual parameters, we studied the variation of misfit as a function of two free parameters, the real part of the element Z_{yx} of

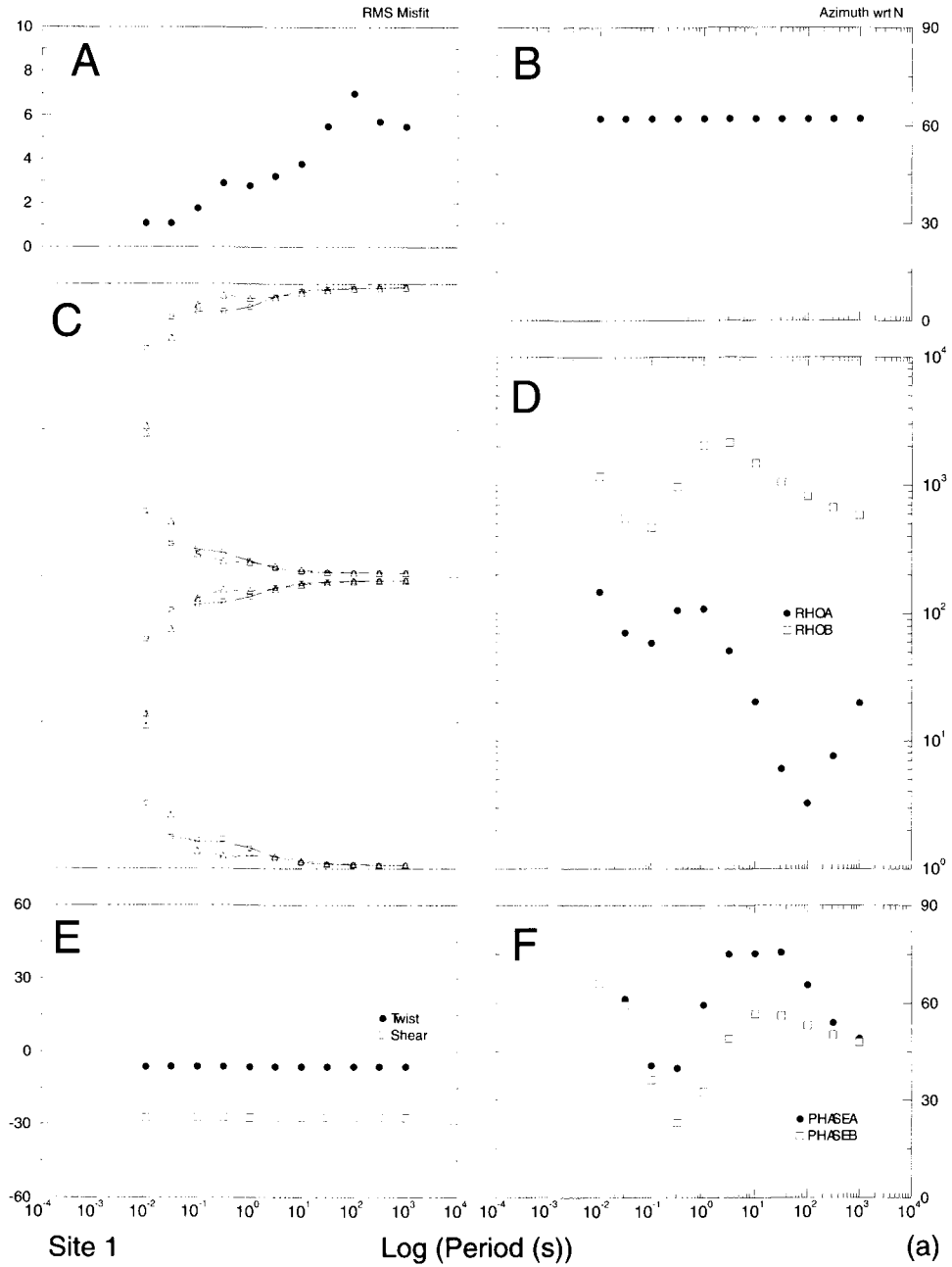
RMS Misfit
Azimuth wrt N
A
B
C
D
E
F
RHOA
RHOB
Twist
Shear
PHASEA
PHASEB
Site 1
Log (Period (s))
(a)

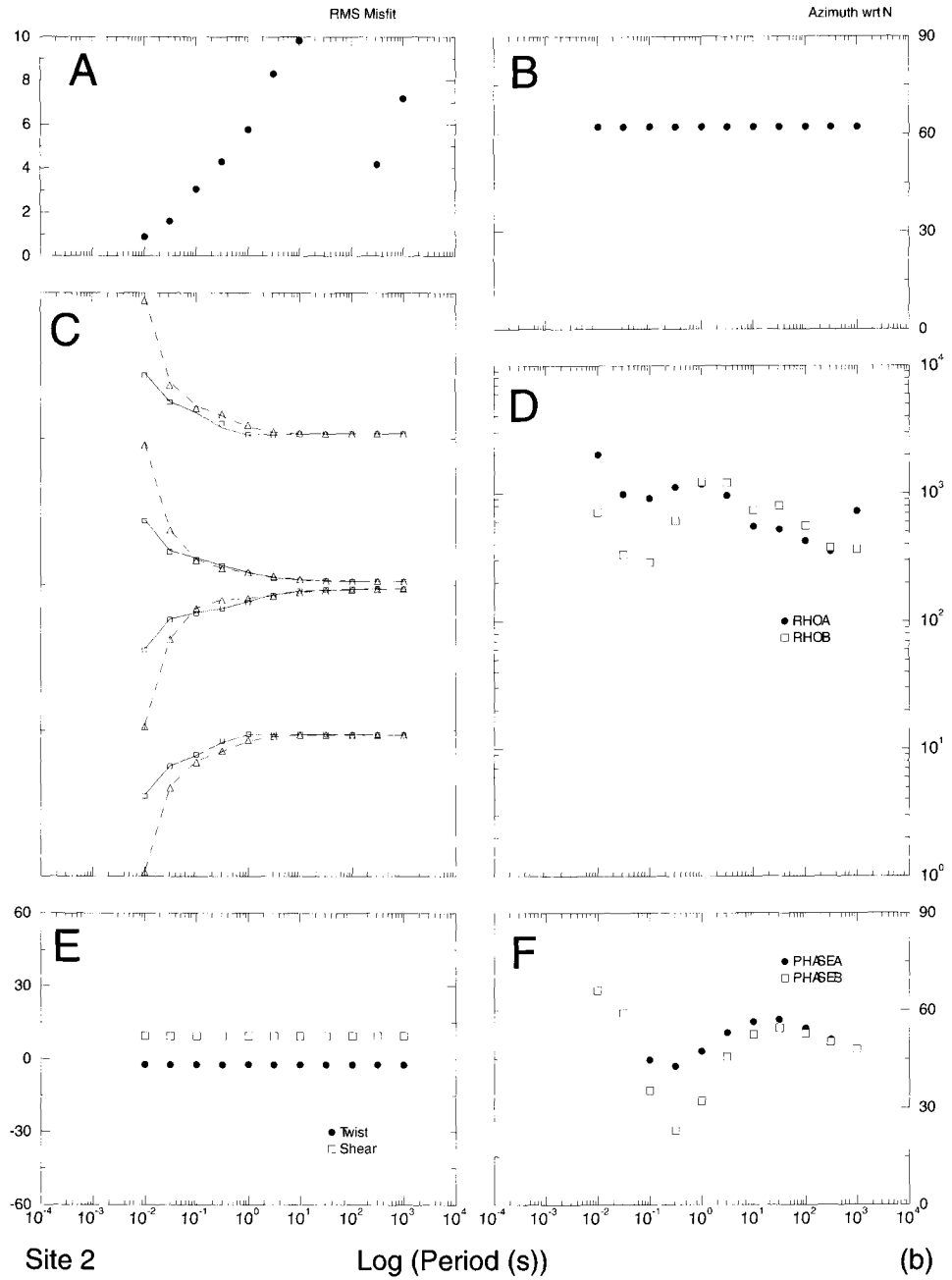

Figure 5. Results from the 2D galvanic decomposition of the stations depicted in Figure 4. (a) Station 1. (b) Station 2. Both figures: A = RMS misfit of the decomposition; B = strike angle; C = impedance fit of the final 2D model to the data; D = regional 2D apparent resistivity; E = twist and shear angles; F = regional 2D phase.

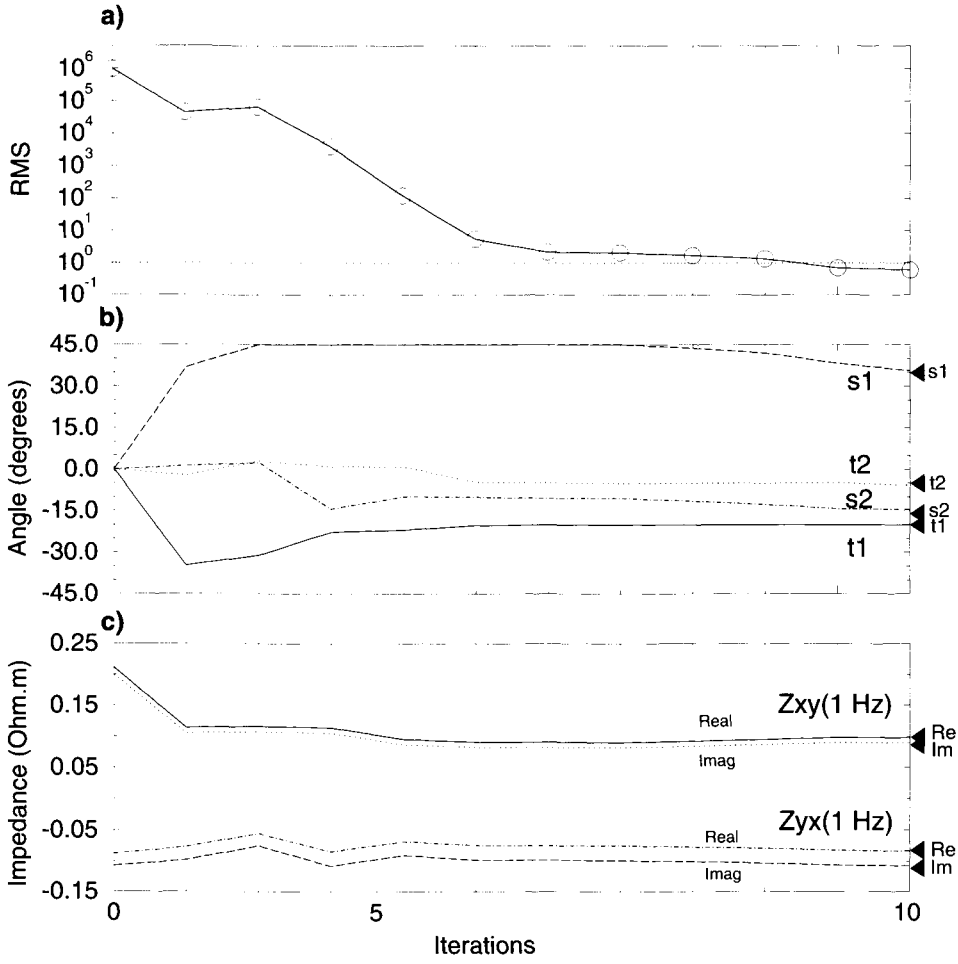

Figure 6. Results corresponding to example 1. (a) RMS misfit. (b) Evolution of the twist and shear angles from an initial value of 0 to their actual values. (c) Evolution of the Z_{xy} and Z_{yx} element of the impedance tensor at a frequency of 1 Hz: continuous line, real part Z_{xy}; dashed line, imaginary part Z_{xy}; dotted line, real part Z_{yx}; dotted–dashed line, imaginary part Z_{yx}. As can be observed, with 10 iterations the correct model is reached.

the regional impedance tensor (at 0.1 Hz) against the shear of the first site, as the other parameters are held constant. Figure 9a shows the variation of the RMS objective function (Equation 13.11) as the two free parameters are varied with all other parameters held at their *correct* values. As can be appreciated, the contoured minimum indicates the correct values for the two parameters (shown by the white cross). In Figure 9b we again contour the misfit against the two free parameters, but in this case the fixed parameters are held to the best-fit values found from our unconstrained procedure. As can be observed in this figure, the minimum is located far from the true solution (black cross), for a shear angle of 45°, but the RMS misfit is still statistically acceptable. Comparison

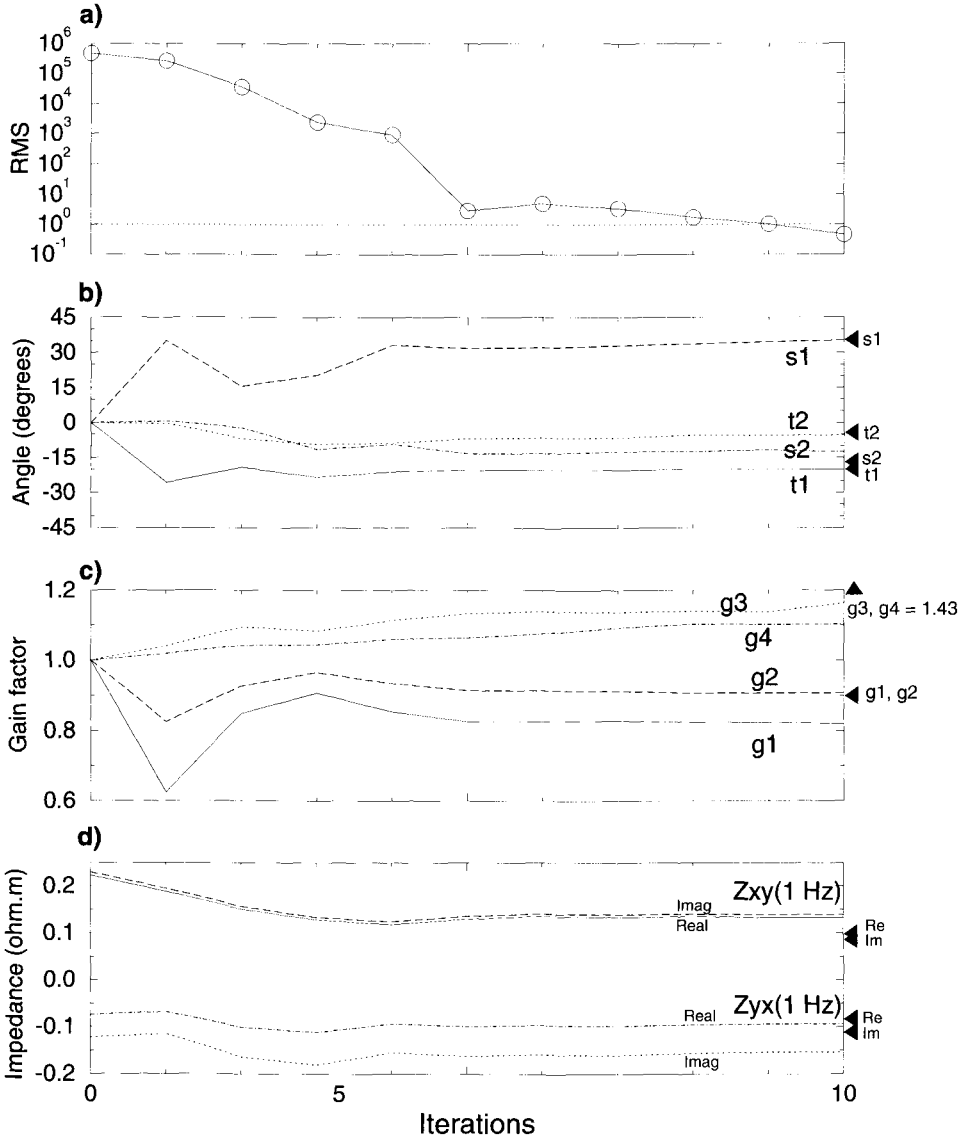

Figure 7. Results corresponding to example 2. (a) RMS misfit. (b) Evolution of the shear and twist angles: continuous line, twist site 1; dashed line, shear site 1; dotted line, twist site 2; dotted–dashed line, shear site 2. (c) Evolution of the gain parameters from an initial value of 1: continuous line, first gain factor site 1; dashed line, second gain factor site 1; dotted line, first gain factor site 2; dotted–dashed line, second gain factor site 2. (d) Evolution of the Z_{xy} and Z_{yx} impedance components at a frequency 1 Hz: continuous line, real part Z_{xy}; dashed line, imaginary part Z_{xy}; dotted line, real part Z_{yx}; dotted–dashed line, imaginary part Z_{yx}.

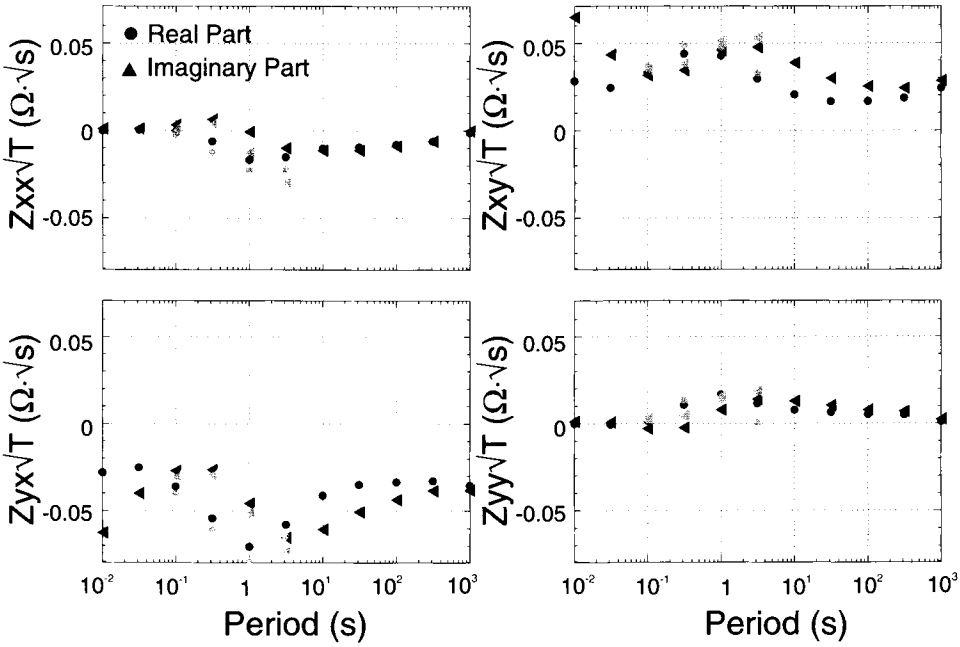

Figure 8. Comparison of the regional impedance tensor scaled by the square of the period from test 2 (in gray) and the theoretical regional values (black).

of Figure 9a and b also indicates that the regional impedances may be more stable and robustly determined than the distortion parameters. However, further work needs to be done to establish whether this is a generic feature, or only one resulting from our choice of impedance tensor and distortion parameters.

5. DISCUSSION

We have developed a 3D/3D decomposition approach for removing 3D galvanic distortion of a 3D regional response. For this purpose we use two adjacent stations and consider that both are sufficiently close to have the same regional 3D response but that they are affected differently by galvanic effects. The decomposition is undertaken in the frequency band where the inductive and magnetic galvanic effects due to the 3D scattering structure vanish.

Using a decomposition scheme similar to that of Groom and Bailey (1989), but with a different parameterization, we can solve the problem. As in the Groom and Bailey case the problem becomes unstable when we try to solve for the site gains, although they can be recovered in our case under some circumstances.

In this work we show that the 2D decomposition technique fails to retrieve the regional model from two three-dimensional sites affected by galvanic distortion. As a consequence, a 2D interpretation of these data would display erroneous features.

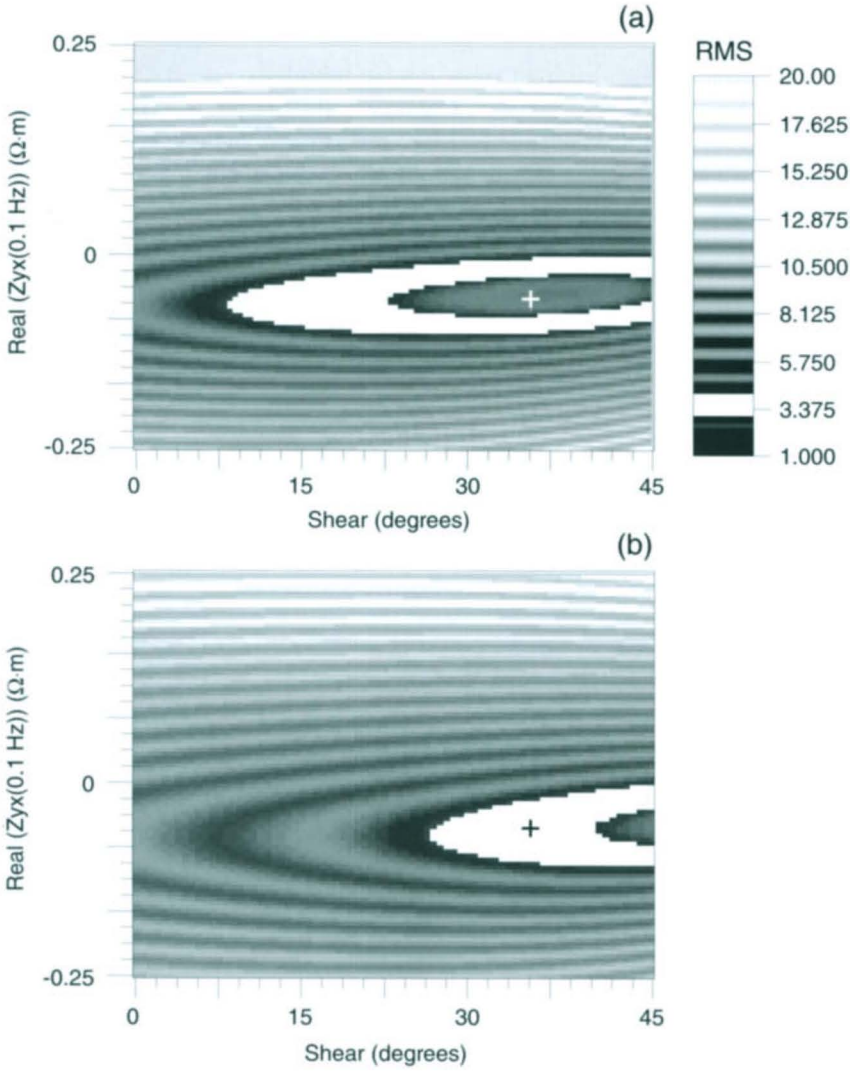

Figure 9. Analysis of the RMS misfit as a function of two parameters (real part of the impedance tensor Z_{yx} at 0.1 Hz and the shear angle from station 1) fixing the rest. (a) The fixed parameters are equal to their actual values. (b) The fixed parameters have been obtained from the inversion of the data. The white area shows the RMS values between 3 and 4. The crosses indicate the location of the true minimum.

The current work is focused on finding a more stable algorithm and a new parameterization of the decomposition equations that allow us to solve the total problem. The addition of the tipper vector to the problem is not advised, as this will add four more equations for each frequency to the problem, but at the same time it will add $4 \times N + 2$ more unknowns: two complex regional tipper per frequency and two vertical magnetic field distortion parameters Q_z to the number of unknowns.

ACKNOWLEDGEMENTS

XG is supported by an industry-GSC research fellowship, and thanks the GSC, Geosystem, Phoenix and Inco for his support. Comments by Jim Craven, Juanjo Ledo, John Weaver, Alan Chave, Phil Wannamaker, Martyn Unsworth and an anonymous reviewer are also acknowledged. Geological Survey of Canada contribution number 2000227.

REFERENCES

Bahr, K., 1991. Geological noise in magnetotelluric data: a classification of distortion types. Phys. Earth Planet. Int., 60, 119–127.

Chave, A.D. and Smith, J.T., 1994. On electric and magnetic galvanic distortion tensor decompositions. J. Geophys. Res., 94, 14,215–14,225.

Garcia, X., Boerner, D. and Pedersen, L.B., 2000. Full galvanic decomposition of tensor CSAMT data. Application to data from the Buchans mine (Newfoundland). Geophys. J. Int., submitted.

Groom, R.W. and Bailey, R.C., 1989. Decomposition of magnetotelluric impedance tensors in the presence of local three-dimensional galvanic distortion. J. Geophys. Res., 94, 1913–1925.

Habashy, T.M., Groom, R.W. and Spies, B.R., 1993. Beyond the Born and Rytov approximations: A nonlinear approach to electromagnetic scattering. J. Geophys. Res., 98, 1759–1776.

Jiracek, G.R., 1990. Near-surface and topographic distortions in EM induction. Surv. Geophys., 11, 163–203.

Jones, A.G. and Groom, R.W., 1993. Strike angle determination from the magnetotelluric tensor in the presence of noise and local distortion: rotate at your peril! Geophys. J. Int., 113, 524–534.

Larsen, J., 1977. Removal of local surface conductivity effects from low frequency mantle response curves. Acta Geodaet., Geophys., Montanist. Acad. Sci. Hung., 12, 183–186.

Ledo, J., Queralt, P. and Pous, J., 1998. Effects of galvanic distortion on magnetotelluric data over a three-dimensional regional structure. Geophys. J. Int., 132, 295–301.

Li, X., Oskooi, B. and Pedersen, L.B., 2000. Inversion of controlled-source tensor magnetotelluric data for a layered earth with azimuthal anisotropy. Geophysics, 65, 452–464.

Mackie, R.L., Smith, J.T. and Madden, T.R., 1994. Three-dimensional electromagnetic modeling using finite difference equations: the magnetotelluric example. Radio Sci., 29(4), 923–935.

McNeice, G.W. and Jones, A.G., 2001. Multi-site, multi-frequency tensor decomposition of magnetotelluric data. Geophysics, 66, 158–173.

Pedersen, L.B. and Rasmussen, T.M., 1989. Inversion of magnetotelluric data: a non-linear least-squares approach. Geophys. Prospect., 37, 669–695.

Qian, W. and Pedersen, L.B., 1992. Near-surface distortion effects on controlled source magnetotelluric transfer functions. Geophys. J. Int., 108, 833–847.

Ritter, P. and Banks, R.J., 1998. Separation of local and regional information in distorted GDS response functions by hypothetical event analysis. Geophys. J. Int., 135, 923–942

Smith, J.T., 1997. Estimating galvanic-distortion magnetic fields in magnetotellurics. Geophys. J. Int., 130, 65–72.

Utada, H. and Munekane, H., 2000. On galvanic distortion of regional three-dimensional magnetotelluric impedances. Geophys. J. Int., 140, 385–398.

Wannamaker, P.E., Hohmann, G.W. and Ward, S.H., 1984. Magnetotelluric responses of three dimensional bodies in layered earth. Geophysics, 49, 1517–1533.

Zhang, P., Pedersen, L.B., Mareschal, M. and Chouteau, M., 1993. Channelling contributions to tipper vectors: a magnetic equivalent to electrical distortion. Geophys. J. Int., 113, 693–700.